

Hybrid computational approach for nonlinear bending of bio-inspired helicoid composite plates using MITC3i and ANN

Huu Trong Dang^{a*} and Quoc Hoa Pham^b

^aFaculty of Mechanical Engineering Technology, Vinh Long University of Technology Education, Vinh Long, Viet Nam

^bFaculty of Fundamental Engineering, Tran Dai Nghia University, Ho Chi Minh City, Vietnam

ARTICLE INFO

Article history:

Received 18 August 2025

Accepted 12 November 2025

Available online

12 November 2025

Keywords:

MITC3i

BiHLCo

FSDT

Pasternak foundation

ANN

ABSTRACT

This paper explores the nonlinear static response of bio-inspired helicoidal laminated composite (BiHLC) plates supported by a Pasternak medium. A combined analytical framework is established by integrating the mixed interpolation of tensorial components (MITC3i) approach with the first order shear deformation plate theory (FSDT). The Pasternak foundation is characterized by its spring stiffness k_1 and shear stiffness k_2 . Based on the Lagrangian energy principle and von Kármán nonlinear theory, the governing equations are formulated and numerically solved through the Newton–Raphson iterative procedure. The effectiveness of the novel method is verified through comparisons with published documents. Additionally, the effects of helicoidal stacking sequences, geometric configurations, boundary constraints, and foundation rigidity on the large deflection behavior are analyzed. An artificial neural network (ANN) model is also proposed to estimate displacements efficiently, eliminating the dependence on finite element computations.

© 2026 Growing Science Ltd. All rights reserved.

1. Introduction

Bio-inspired helicoid laminated composites (BiHLCo) are an advanced class of materials inspired by the complex designs found in nature. These materials simulate the helical structures observed in biological systems such as shells, bones, and other natural composite materials that are highly durable and resistant to damage. By simulating these natural structures, engineers aim to develop new composite materials that combine lightness with improved mechanical properties, such as strength, stiffness, and resilience under various loading conditions. These structures are created by layering materials in a helical tyle, which optimizes load distribution and improves the overall performance of the material under stress (Benyus, 1997).

The BiHLCo structures in nature provide an optimal arrangement for force distribution, resulting in improved material response when subjected to bending, tensile, or compression forces. The combination of organic and inorganic materials in biocomposites, such as the arrangement of collagen fibers and minerals in bone, has inspired the development of similar composite materials in engineering. These bioinspired materials not only improve the strength and flexibility of composites but also contribute to their sustainability by using natural and abundant resources for reinforcement (Barbero, 2011). In addition, bioinspired materials can reduce the environmental impact of their production by using low-energy processes and incorporating waste materials or natural components.

Recent studies have increasingly focused on the application of bioinspired designs to develop advanced materials with improved performance, particularly in fields such as aerospace, civil engineering, and automotive industries (Pawlyn, 2019). Garg et al., (2023) presented the finite element analysis (FEM) to examine the natural vibration response of BiHLCo plates, utilizing a higher order zigzag theory. Sharma et al., (2023) applied a shear deformation theory based on Navier solutions to study the bending response of BiHLCo structures inspired by biological helicoids. Karamanli et al., (2024) utilized a quasi-

* Corresponding author.

E-mail addresses: trongdh@vlute.edu.vn (H.T. Dang)

ISSN 2291-8752 (Online) - ISSN 2291-8744 (Print)

© 2026 Growing Science Ltd. All rights reserved.

doi: 10.5267/j.esm.2025.11.002

3D kinematic plate theory within a FEM framework to perform the bending, buckling, and natural vibration analyses of BiHLCo plates with various layup configurations. Amara et al., (2024) developed an analytical solution relied on the deformation compatibility to assess the effects of thermo-hygroscopic conditions and moisture on BiHLCo plates, with applications in strengthening damaged reinforced concrete beams. Mohamed et al., (2022a) explored the static, buckling, and vibration responses of BiHLCo plates through a two-dimensional differential quadrature method, leveraging the FSDT. In addition, Do et al., (2023) employed an iso-geometric analysis framework incorporating higher-order shear deformation theory (HSDT) and Soldatos's continuous function to investigate the natural vibration characteristics of BiHLCo plates supported by elastic foundations.

Recently, the improvement of triangular elements in the FEM Mohammad Malekzadeh, (2021) has garnered significant attention from researchers and scientists worldwide. This growing interest stems from the critical role that triangular elements play in solving complex engineering and scientific problems. As a fundamental building block in mesh generation, triangular elements are widely used due to their flexibility in modeling irregular geometries and their suitability for adaptive meshing techniques. However, challenges related to accuracy, convergence, and computational efficiency have prompted extensive studies to optimize their performance. Lee and Bathe (2004, 2010) introduced a straightforward technique for designing isotropic triangular shell finite elements, utilizing the MITC framework. Lee et al., (2014, 2015) developed the MITC3+ method, a novel finite element with three node triangular element, for effective modeling of isotropic shell structures. Nguyen et al., (2016) enhanced the MITC3 triangular element for applications in static bending and natural vibration analyses of functionally graded (FG) sandwich plates. Bischoff & Bletzinger (2004) proposed stabilized FEM techniques to address Reissner/Mindlin plate challenges. Cui and Tian (2017) advanced the discrete shear gap methodology, centered on a three-node triangular element, for analyzing both linear and geometrically nonlinear behaviors of plates and shells. Some researchers such as (Pham et al., 2019, 2022a,b, 2023) applied an edge smoothing approach in combination with the MITC interpolation method for triangular elements, enabling the analysis of plates and shells constructed from advanced smart materials. In recent years, the rapid growth of computational mechanics has encouraged the integration of traditional finite element methods with modern data-driven approaches. This trend has led to the increasing adoption of Artificial Intelligence (AI) techniques to improve computational efficiency, enhance predictive accuracy, and accelerate design optimization.

In today's world, the use of artificial intelligence (AI) in solving mechanical problems has drawn significant interest from researchers, with ANN models standing out as a key approach. Some recent notable studies for structures using smart material by Khatir et al., (2021) introduced a two-stage methodology for investigating damage detection, localization, and quantification in FGM plate structures. The FEM and ANN approaches are employed to analyze the bending static parameters, including stresses and potentials, of a smart sandwich plate featuring a porous nanocomposite core reinforced with agglomerated carbon nanotubes and piezo-magneto-thermo-electric facings by Mahesh (2023). Fadlallah et al., (2021) presented a simulation–optimization framework for predicting behavior and optimizing the structure of lightweight honeycomb sandwich composite heliostats, incorporating the ANN technique and the PSO algorithm. Ribeiro Junior & Gomes (2023) conducted a review of the most significant and recent studies on machine learning methods for damage evaluation in laminate composite structures.

Despite the extensive studies mentioned above, the MITC3i element has not yet been employed for analyzing composite plates. This paper introduces a novel investigation into the nonlinear static bending behavior of BiHLCo plates relied on a Pasternak medium using MITC3i and ANN. Within the framework of small strain theory and moderate rotations, the nonlinearity is modeled using von Kármán's large deflection theory, and the nonlinear equilibrium equations are solved utilizing the Newton–Raphson algorithmic procedure. To validate the proposed approach, several numerical examples are presented, showcasing its effectiveness in comparison with methods available in the literature. Following the verification of accuracy and efficiency, this study further explores the influence of geometric characteristics, material characteristics, foundation models, and boundary constraints on the nonlinear bending response of BiHLCo plates supported by elastic foundations. Furthermore, an ANN-based prediction method for rapidly estimating the nonlinear displacement of BiHLCo composite plates. The proposed model ensures high accuracy while significantly reducing computational costs, paving the way for broader ANN applications in structural analysis.

The content of this paper is arranged as follows: Section 1 introduces previous studies on related issues. Section 2 presents the formulations for BiHLCo plates. In Section 3, the finite element formulation using MITC3i is introduced. Section 4 provides various numerical examples to validate and assess the performance of the proposed FEM and ANN model. Finally, Section 5 concludes with remarks and insights.

2. Formulations of BiHLC plates

2.1. The BiHLCo plate on Pasternak medium

This study investigates BiHLCo plates featuring various stacking configurations. The detailed layouts are illustrated in **Fig. 1** and **Fig. 2**, while their specifications are conveniently summarized in **Table 1**.

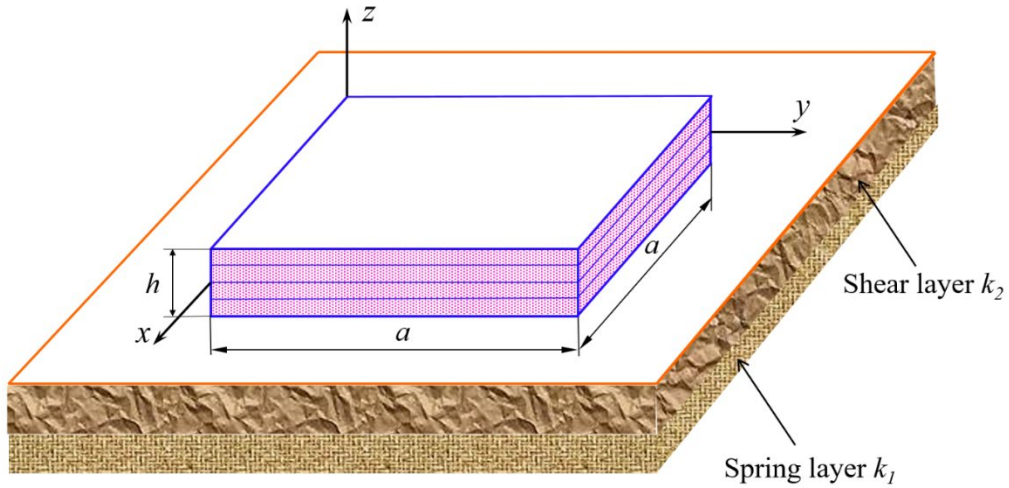


Fig. 1. The BiHLCo plate is modeled on an elastic medium

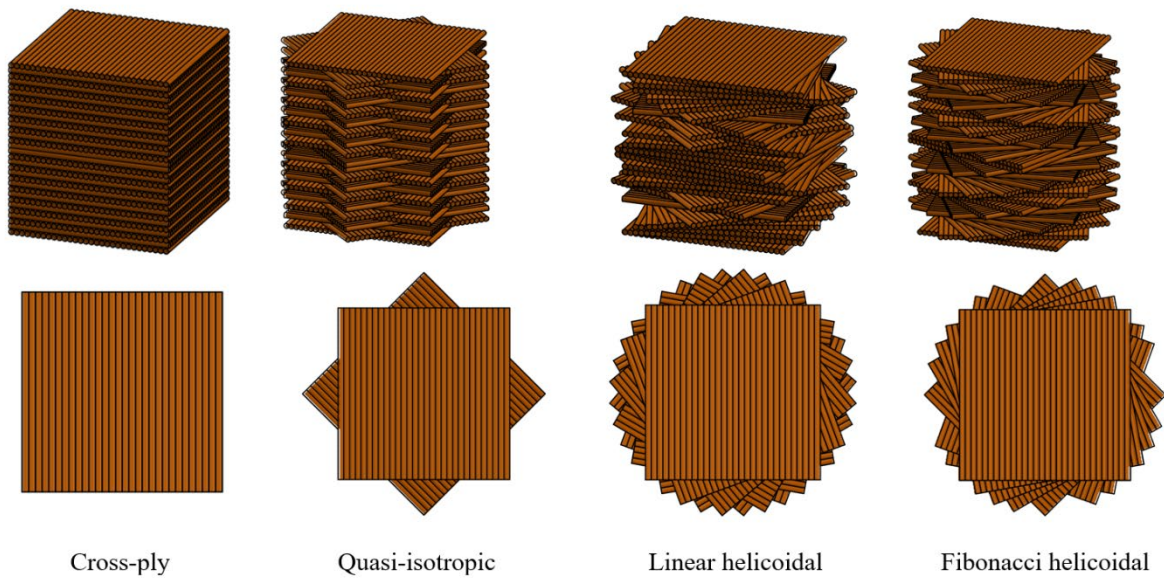


Fig. 2. Different lay-up configurations of BiHLCo plates

Table 1. Specifications of the layers of BiHLCo

Label	N_L	Lay-up sequence	Rephrased Description
UD	32	$[0^\circ/0^\circ \dots 0^\circ/0^\circ]$	Layers oriented in a single fiber direction (unidirectional).
QI	32	$[0^\circ/45^\circ/90^\circ/-45^\circ]_{4s}$	Symmetric quasi-isotropic stacking that balances stiffness in multiple directions.
CP	32	$[0^\circ/90^\circ]_{8s}$	Alternating orthogonal layers forming a symmetric cross-ply layout.
FH	32	$[0^\circ/10^\circ/10^\circ/20^\circ/30^\circ/50^\circ/80^\circ/130^\circ/210^\circ/340^\circ/190^\circ/170^\circ/360^\circ/170^\circ/170^\circ/340^\circ]$	Fibonacci-based helicoidal stacking following a quasi-natural angular progression.
LH	32	$[0^\circ/24^\circ \dots 360^\circ]_s$	Linear helicoidal stacking sequence with 24° angular increment between adjacent plies.

2.2. The correlation between the displacement, stress, and strain fields in BiHLCo plates

The displacement field of BiHLCo plates, as determined based on the FSDT, is represented by

$$\begin{cases} u(x, y, z) = u_0(x, y) + z\varphi_x(x, y) \\ v(x, y, z) = v_0(x, y) + z\varphi_y(x, y), \\ w(x, y, z) = w_0(x, y) \end{cases} \quad (1)$$

where u_0, v_0, w_0 are displacement variables in x, y and z directions; φ_x, φ_y are the rotations in the xz and yz plane, respectively.

Following the determination of the plate's displacement fields, we can completely determine the strain field as follows:

$$\boldsymbol{\varepsilon} = \boldsymbol{\varepsilon}_m + z\boldsymbol{\kappa} \quad (2)$$

where

The strain on the membrane $\boldsymbol{\varepsilon}_m$ following von Kármán theory is:

$$\boldsymbol{\varepsilon}_m = \boldsymbol{\varepsilon}_m^L + \boldsymbol{\varepsilon}_m^{NL} = \begin{Bmatrix} u_{0,x} \\ v_{0,y} \\ u_{0,y} + v_{0,x} \end{Bmatrix} + \frac{1}{2} \begin{Bmatrix} w_{,x}^2 \\ w_{,y}^2 \\ 2w_{,x}w_{,y} \end{Bmatrix} \quad (3)$$

in which $\boldsymbol{\varepsilon}_m^{NL}$ is nonlinear membrane strain and can be re-written by

$$\boldsymbol{\varepsilon}_m^{NL} = \frac{1}{2} \begin{Bmatrix} w_{,x}^2 \\ w_{,y}^2 \\ 2w_{,x}w_{,y} \end{Bmatrix} = \frac{1}{2} \begin{bmatrix} w_{,x} & 0 \\ 0 & w_{,y} \\ w_{,y} & w_{,x} \end{bmatrix} \begin{bmatrix} w_{,x} \\ w_{,y} \end{bmatrix} = \frac{1}{2} \mathbf{C}\mathbf{Y} \quad (4)$$

The bending strain $\boldsymbol{\kappa}$ is:

$$\boldsymbol{\kappa} = \begin{Bmatrix} \varphi_{x,x} \\ \varphi_{y,y} \\ \varphi_{x,y} + \varphi_{y,x} \end{Bmatrix} \quad (5)$$

The shear strain across the transverse $\boldsymbol{\gamma}$ is:

$$\boldsymbol{\gamma} = \begin{Bmatrix} w_{,x} + \varphi_x \\ w_{,y} + \varphi_y \end{Bmatrix} \quad (6)$$

The constitutive relations for each ply are transformed from the local material axes to the global coordinate frame, as the BiHLCo plate consists of multiple orthotropic laminae, each exhibiting its own elastic characteristics. The h -th layer's stress-strain relationships in laminate coordinates are provided by

$$\boldsymbol{\sigma}_m = \begin{Bmatrix} \sigma_{xx} \\ \sigma_{yy} \\ \tau_{xy} \end{Bmatrix} = \begin{bmatrix} \bar{Q}_{11} & \bar{Q}_{12} & \bar{Q}_{16} \\ \bar{Q}_{21} & \bar{Q}_{22} & \bar{Q}_{26} \\ \bar{Q}_{61} & \bar{Q}_{62} & \bar{Q}_{66} \end{bmatrix}^{(k)} \begin{Bmatrix} \varepsilon_x \\ \varepsilon_y \\ \gamma_{xy} \end{Bmatrix} = \bar{\mathbf{Q}}_m (\boldsymbol{\varepsilon}_m + z\boldsymbol{\kappa}) \quad (7)$$

$$\boldsymbol{\tau}_s = \begin{Bmatrix} \tau_{xz} \\ \tau_{yz} \end{Bmatrix} = \begin{bmatrix} \bar{Q}_{44} & \bar{Q}_{45} \\ \bar{Q}_{54} & \bar{Q}_{55} \end{bmatrix}^{(k)} \begin{Bmatrix} \gamma_{xz} \\ \gamma_{yz} \end{Bmatrix} = \bar{\mathbf{Q}}_s \boldsymbol{\gamma}_s \quad (8)$$

where \bar{Q}_{ij} denote the transformed stiffness coefficients obtained from the coordinate transformation, as presented by (Mohamed et al., 2022b).

$$\bar{\mathbf{Q}} = \mathbf{T}_\sigma^{-1} \mathbf{Q} \mathbf{T}_\varepsilon \quad (9)$$

where \mathbf{T}_σ^{-1} and \mathbf{T}_ε are the stress-strain transformation matrices defined by the rotation angle θ :

$$\mathbf{T}_\sigma = \begin{bmatrix} C^2 & S^2 & 2CS \\ S^2 & C^2 & -2CS \\ -CS & CS & C^2 - S^2 \end{bmatrix}, \mathbf{T}_\varepsilon = \begin{bmatrix} C^2 & S^2 & 2CS \\ S^2 & C^2 & -2CS \\ -2CS & 2CS & C^2 - S^2 \end{bmatrix}$$

here, $S = \sin\theta$, $C = \cos\theta$; θ is the orientation angle between the global x -axis and the local material axis x_1 . The terms Q_{ij} denote the reduced stiffness coefficients evaluated in the material coordinate frame, and are given by:

$$Q_{11} = \frac{E_{11}}{1 - \nu_{12}\nu_{21}}, Q_{22} = \frac{E_{22}}{1 - \nu_{12}\nu_{21}}, Q_{12} = \frac{\nu_{12}E_{22}}{1 - \nu_{12}\nu_{21}} \quad (10)$$

$$Q_{44} = G_{23}, Q_{66} = G_{12}, Q_{55} = G_{13}$$

here, E_{11} and E_{22} denote the longitudinal and transverse Young's moduli, respectively; ν_{12} and ν_{21} correspond to Poisson's ratios; and G_{12} , G_{13} and G_{23} are the shear moduli in the respective planes.

2.3. The governing equation

The Lagrange energy function defines the primary equation governing sandwich plates as in Ref. Reddy, (2003):

$$\Pi = U + V + U^f \quad (11)$$

here, U and V represent the strain energy and potential energy of BiHLCo, respectively, while U^f represents the strain energy stored in the elastic medium. The expression for the strain energy of BiHLCo is given as:

$$U = \frac{1}{2} \int_{\Theta} (\boldsymbol{\sigma}_m^T \boldsymbol{\varepsilon}_m + z \boldsymbol{\sigma}_m^T \boldsymbol{\kappa} + \boldsymbol{\tau}_s^T \boldsymbol{\gamma}_s) d\Theta \quad (12)$$

$$= \frac{1}{2} \int_{\Omega} (\boldsymbol{\varepsilon}_m^T \mathbf{A} \boldsymbol{\varepsilon}_m + \boldsymbol{\kappa}^T \mathbf{B} \boldsymbol{\varepsilon}_m + \boldsymbol{\varepsilon}_m^T \mathbf{B} \boldsymbol{\kappa} + \boldsymbol{\varepsilon}_m^T \mathbf{D} \boldsymbol{\varepsilon}_m + \boldsymbol{\gamma}_s^T \mathbf{D}_s \boldsymbol{\gamma}_s) d\Omega$$

with Θ and Ω are the volume and area of the plate and the stiffness matrices \mathbf{A} , \mathbf{B} , \mathbf{D} and \mathbf{D}_s are expressed as follows:

$$(\mathbf{A}, \mathbf{B}, \mathbf{D}) = \int_{-h/2}^{h/2} (1, z, z^2) \bar{\mathbf{Q}}_m dz \quad (13)$$

$$\mathbf{D}_s = \frac{5}{6} \int_{-h/2}^{h/2} \bar{\mathbf{Q}}_s dz \quad (14)$$

The strain energy variation of the foundation is represented by the equation below:

$$U^f = \int_{\Omega} R w d\Omega \quad (15)$$

The work performed by a uniformly distributed transverse load is expressed as:

$$V = - \int_{\Omega} p w d\Omega. \quad (16)$$

The Lagrange energy functional is now reformulated as:

$$\Pi = \frac{1}{2} \int_{\Omega} ((\boldsymbol{\varepsilon}_m^L + \boldsymbol{\varepsilon}_m^{NL})^T \mathbf{A} (\boldsymbol{\varepsilon}_m^L + \boldsymbol{\varepsilon}_m^{NL}) + \boldsymbol{\kappa}^T \mathbf{B} (\boldsymbol{\varepsilon}_m^L + \boldsymbol{\varepsilon}_m^{NL}) + (\boldsymbol{\varepsilon}_m^L + \boldsymbol{\varepsilon}_m^{NL})^T \mathbf{B} \boldsymbol{\kappa} + (\boldsymbol{\varepsilon}_m^L + \boldsymbol{\varepsilon}_m^{NL})^T \mathbf{D} (\boldsymbol{\varepsilon}_m^L + \boldsymbol{\varepsilon}_m^{NL}) + \boldsymbol{\gamma}_s^T \mathbf{D}_s \boldsymbol{\gamma}_s) d\Omega + \int_S R w dS - \int_S p w dS \quad (17)$$

3. Finite element formulation using MITC3i

3.1. Kinematic equations

The BiHLC plate's mid-plane is subdivided into n^e triangular elements of the MITC3i type, each consisting of n^n nodes, such that the overall region Ω is approximately the sum of individual elements Ω_e , with no overlapping between elements ($\Omega_i \cap \Omega_j = \emptyset, i \neq j$). The displacement field across each element Ω_e can be written as $\mathbf{u}^e = \sum_{j=1}^{n^e} \mathbf{N}_j(x) \mathbf{d}_j^e$. Where \mathbf{N}_j is the matrix of shape functions corresponding to the j -th node, and \mathbf{d}_j^e represents the vector of nodal degrees of freedom (DOFs). The vector \mathbf{u}^e collects all the element's translation and rotation degrees of freedom (Lee et al., 2014). The in-plane and bending deformation components of the MITC3i element are calculated using the following expressions:

$$\boldsymbol{\varepsilon}_m^L = \mathbf{B}_m^L \mathbf{d}, \quad (18)$$

$$\boldsymbol{\varepsilon}_m^{NL} = \frac{1}{2} \mathbf{B}_m^{NL} \mathbf{d}, \quad (19)$$

$$\boldsymbol{\kappa} = \mathbf{B}_b \mathbf{d}, \quad (20)$$

where

$$\mathbf{B}_m^L = \begin{bmatrix} \frac{\partial N_i}{\partial x} & 0 & 0 & 0 & 0 \\ 0 & \frac{\partial N_i}{\partial y} & 0 & 0 & 0 \\ \frac{\partial N_i}{\partial y} & \frac{\partial N_i}{\partial x} & 0 & 0 & 0 \end{bmatrix}, \quad (21)$$

$$\mathbf{B}_m^{NL} = \mathbf{C} \mathbf{G} \quad (22)$$

$$\mathbf{G} = \begin{bmatrix} 0 & 0 & \frac{\partial N_i}{\partial x} & 0 & 0 \\ 0 & 0 & \frac{\partial N_i}{\partial y} & 0 & 0 \end{bmatrix}, \quad (23)$$

and

$$\mathbf{B}_b = \begin{bmatrix} 0 & 0 & 0 & \frac{\partial N_i}{\partial x} & 0 \\ 0 & 0 & 0 & 0 & \frac{\partial N_i}{\partial y} \\ 0 & 0 & 0 & \frac{\partial N_i}{\partial y} & \frac{\partial N_i}{\partial x} \end{bmatrix}, \quad (24)$$

with N_i denotes the shape function for MITC3i triangular element. In order to address the shear locking issue in triangular elements, the authors proposed a mathematical model utilizing the shear strain from MITC3i theory, which is expressed as:

$$\boldsymbol{\gamma} = \mathbf{B}_s \mathbf{d}, \quad (25)$$

in which \mathbf{B}_s is the transverse shear strain that is approximated to avoid shear locking, as presented by Lee et al. (2014). Substituting the strain fields into equation (17), to describe the behavior of the BiHLCo plate, the following general equation can be written:

$$\mathbf{K} \mathbf{d} = \mathbf{F} \quad (26)$$

In this equation, the global stiffness matrix \mathbf{K} can be expressed as the combination of several components, namely: the linear part (\mathbf{K}_L), the nonlinear part (\mathbf{K}_{NL}), the geometric stiffness matrix (\mathbf{K}_G), and the elastic medium stiffness matrix (\mathbf{K}_F). Each of these matrices represents a distinct physical effect within the overall structural response. Accordingly, the stiffness matrices are obtained from the element contributions as follows:

$$\mathbf{K}_L = \sum_1^{ne} \mathbf{K}_L^e, \mathbf{K}_G = \sum_1^{ne} \mathbf{K}_G^e, \mathbf{K}_{NL} = \sum_1^{ne} \mathbf{K}_{NL}^e, \text{ and } \mathbf{K}_F = \sum_1^{ne} \mathbf{K}_F^e \quad (27)$$

here, ne denotes the sum of all elements in the discretized domain. The global matrices are assembled by combining the respective element matrices using the FEM. Each element matrix represents the interaction of various physical factors of the plate, including linear stiffness, nonlinear stiffness, geometric stiffness, and the effects of the foundation. For the load vector, the global load \mathbf{F} can be expressed as the sum of the loads of each individual element:

$$\mathbf{F} = \sum_1^{ne} \mathbf{p}^e \quad (28)$$

For the linear stiffness matrix \mathbf{K}_L^e , it includes characteristic components as shown below:

$$\mathbf{K}_L^e = \mathbf{K}_{Lb}^e + \mathbf{K}_{Ls}^e = \int_{\Omega} \left[(\mathbf{B}_m^L)^T \mathbf{A} \mathbf{B}_m^L + (\mathbf{B}_m^L)^T \mathbf{B} \mathbf{B}_b + (\mathbf{B}_b)^T \mathbf{B} \mathbf{B}_m^L + (\mathbf{B}_b)^T \mathbf{D} \mathbf{B}_b \right] d\Omega + \int_{\Omega} (\mathbf{B}_s)^T \mathbf{D}_s \mathbf{B}_s d\Omega \quad (29)$$

$$\mathbf{K}_{NL}^e = \int_{\Omega} \left[\frac{1}{2} (\mathbf{B}_m^L)^T \mathbf{A} \mathbf{B}_m^{NL} + (\mathbf{B}_m^{NL})^T \mathbf{A} \mathbf{B}_m^L + \frac{1}{2} (\mathbf{B}_m^{NL})^T \mathbf{A} \mathbf{B}_b \right] d\Omega \quad (30)$$

$$\mathbf{K}_G^e = \int_{\Omega} \mathbf{G}^T \mathbf{N} \mathbf{G} d\Omega \quad (31)$$

with

$$\mathbf{N} = \begin{bmatrix} N_x & N_{xy} \\ N_{xy} & N_y \end{bmatrix} \text{ with } (N_x, N_y, N_{xy}) = \int_{-h/2}^{h/2} (\sigma_x, \sigma_y, \sigma_{xy}) dz \quad (32)$$

The foundation element stiffness matrix is:

$$\mathbf{K}_F^e = k_1 \int_{\Omega} \mathbf{N}_w^T \mathbf{N}_w d\Omega + k_2 \int_{\Omega} \left[\left(\frac{\partial \mathbf{N}_w}{\partial x} \right)^T \left(\frac{\partial \mathbf{N}_w}{\partial x} \right) + \left(\frac{\partial \mathbf{N}_w}{\partial y} \right)^T \left(\frac{\partial \mathbf{N}_w}{\partial y} \right) \right] d\Omega \quad (33)$$

where \mathbf{N}_w is defined by

$$\mathbf{N}_w = [0 \quad N_1 \quad 0 \quad \dots \quad 0 \quad N_3 \quad 0] \quad (34)$$

The element load vector is:

$$\mathbf{p}^e = \int_{\Omega} \mathbf{N}_w^T p d\Omega \quad (35)$$

where p is the transverse load.

3.2. Perform the solution procedure for the governing equation

The nonlinear static solution is obtained by solving the following algebraic equation $\mathbf{K}\mathbf{d} = \mathbf{F}$ from Eq. (26). The stiffness matrix \mathbf{K} exhibits a nonlinear dependence on the unknown displacement variable \mathbf{d} , primarily because \mathbf{B}_m^{NL} is a function of the displacement field. Consequently, the nonlinear equilibrium Eq. (26) must be solved iteratively. To facilitate this process, the governing equation is reformulated in terms of the residual force:

$$\boldsymbol{\varphi}(\mathbf{d}) = \mathbf{K}\mathbf{d} - \mathbf{F} \rightarrow 0 \quad (36)$$

The residual force represents the approximation error, which progressively diminishes with each iteration. Given an initial approximation \mathbf{d}^i at the i^{th} iteration, an updated solution is computed at each step.

$$\mathbf{d}^{i+1} = \mathbf{d}^i + \Delta\mathbf{d} \quad (37)$$

where $\Delta\mathbf{d}$ represents the incremental displacement calculated by

$$\boldsymbol{\varphi}(\mathbf{d}^{i+1}) = \boldsymbol{\varphi}(\mathbf{d}^i) + \mathbf{K}^T \Delta\mathbf{d} \quad (38)$$

here, \mathbf{K}^T referred to as the tangent stiffness matrix at the i^{th} iteration, is defined as:

$$\mathbf{K}^T = \frac{\partial \boldsymbol{\varphi}(\mathbf{d}^i)}{\partial \mathbf{d}} = \mathbf{K}_{NL} + \mathbf{K}_G \quad (39)$$

Eq. (37) is iterated until the displacement error between two consecutive iterations meets the specified tolerance, $\varepsilon=0.001$. The Newton-Raphson method is illustrated in the flowchart shown in **Fig. 3**.

$$\frac{|\mathbf{d}^{i+1} - \mathbf{d}^i|}{\mathbf{d}^i} < \varepsilon \quad (40)$$

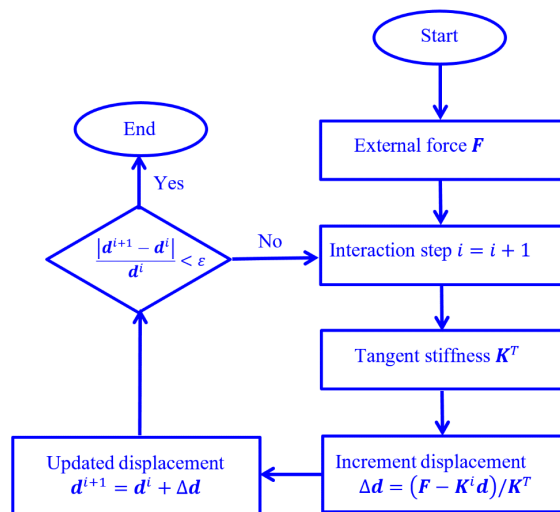


Fig. 3. Diagram for the nonlinear static bending analysis process of a BiHLC_o plate

3.3. Boundary conditions

The model involves three distinct boundary conditions are applied in this problem:

SSSS: Displacement and rotation are fixed at the lower and upper edges: $u_0 = w_0 = \varphi_x = 0$ and $v_0 = w_0 = \varphi_y = 0$ at left and right edges

SSSS1: Displacement and rotation are fixed at the lower and upper edges: $u_0 = v_0 = w_0 = \varphi_x = 0$ at lower and upper edges and $u_0 = v_0 = w_0 = \varphi_y = 0$ at left and right edges

CCCC: All displacements and rotations are fixed at all edges: $u_0 = v_0 = w_0 = \varphi_x = \varphi_y = 0$.

4. Findings and Discussion

4.1. Comparison study

4.1.1. Linear problems

In this subsection, the accuracy and convergence of the current mathematical model and FEM with MITC3 element are compared to the published work in the literature. The material properties for BiHLC_o plates studied here are: $E_1 = 25$, $E_2 = 1$, $G_{12} = G_{13} = 0.5E_2$, $\nu_{12} = 0.25$, $G_{23} = 0.2E_2$. The dimensional parameters of the BiHLC_o plate are given as follows: $a = b = 1$. In some specific examples, the authors will provide the geometric dimensions and material properties of the plate for the readers' convenience. The transverse loading $q(x, y)$ can be presented as:

$$q(x, y) = \begin{cases} q_0 \sin\left(\frac{\pi x}{a}\right) \sin\left(\frac{\pi y}{a}\right) & \text{Sinusoidal distributed load (SDL)} \\ q_0 & \text{Uniform distributed load (UDL)} \end{cases} \quad (41)$$

in which q_0 represents the magnitude of the load. To facilitate comparison of the results with other studies, the non-dimensional displacement values are presented as follows:

$$w = w_0 \left(\frac{a}{2}, \frac{b}{2}\right) \frac{E_2 h^3}{a^4 q_0} \quad (42)$$

Firstly, **Table 2** compares the nondimensional maximum deflection of simply supported BiHLC_o plates under sinusoidal distributed load (SDL) of current work with the results of Mohamed et al., 2022b. Three different thickness-to-length ratios of BiHLC_o plate were investigated $\frac{a}{h} = 10, 20, 100$ and layup changed from UD, CP, QI, LH, and FH. The authors examine the maximum displacement of the plate across various mesh levels, including 8×8 , 12×12 , and 16×16 . As predicted from this table, It is evident that the current results for deflection are identical to those in Mohamed et al., 2022b. It is noted that for different thickness ratios (a/h) and layup configurations, the error of the present method using a 16×16 mesh compared to the results of Mohamed et al., 2022b is always less than 1%. Additionally, we observe that the UD layer results in the greatest displacement, whereas the QI layer gives the smallest.

Table 2. The maximum deflection (w) of SSSS BiHLC_o plate with different values of length-to-thickness ratio subjected to SSL ($\frac{E_1}{E_2} = 25$)

a/h	Method	UD	CP	QI	LH	FH
10	This study 8×8	0.6169	0.5856	0.4749	0.4816	0.5247
		3.353%	3.318%	3.022%	3.235%	3.192%
	This study 12×12	0.6339	0.6007	0.4842	0.4911	0.5362
		0.689%	0.825%	1.123%	1.326%	1.070%
	This study 16×16	0.6400	0.6061	0.4876	0.4945	0.5403
	0.266%	0.066%	0.429%	0.643%	0.314%	
	Mohamed et al., 2022b	0.6383	0.6057	0.4897	0.4977	0.5420
20	This study 8×8	0.4616	0.4557	0.3451	0.3512	0.3899
		4.549%	4.043%	3.845%	3.834%	4.084%
	This study 12×12	0.4782	0.4704	0.3540	0.3602	0.4010
		1.117%	0.948%	1.365%	1.369%	1.353%
	This study 16×16	0.4840	0.4756	0.3571	0.3633	0.4050
	0.083%	0.147%	0.502%	0.520%	0.369%	
	Mohamed et al., 2022b	0.4836	0.4749	0.3589	0.3652	0.4065
100	This study 8×8	0.3974	0.4028	0.2980	0.3038	0.3385
		8.285%	6.975%	5.994%	5.944%	6.698%
	This study 12×12	0.4247	0.4264	0.3111	0.3170	0.3556
		1.985%	1.524%	1.861%	1.858%	1.985%
	This study 16×16	0.4324	0.4331	0.3149	0.3209	0.3606
	0.208%	0.023%	0.662%	0.650%	0.606%	
	Mohamed et al., 2022b	0.4333	0.4330	0.3170	0.3230	0.3628

Table 3 presents nondimensional center deflection of laminate plates resting on elastic medium under SDL. The composite plate with two layer ($0^\circ/90^\circ$), the material properties are $E_1 = 25, E_2 = 1, G_{12} = G_{13} = 0.5E_2, \nu_{12} = 0.25, G_{23} = 0.2E_2$. The plate is placed on a foundation with two parameters K_1 and K_2 . From this table, we can see that the numerical results of the current work are in very well agreement with the results published in the work of Setoodeh & Karami, 2004 at a mesh size of 16×16 . Additionally, we also observe that with the support of the elastic foundation, the displacement of the plate significantly decreases. This can be interpreted as the increase in the stiffness of the plate when an elastic foundation supports the plate.

Table 3. Nondimensional center deflection of laminate plates resting on elastic medium

a/h	Elastic parameters	Method	$w = w_0 \left(\frac{a}{2}, \frac{b}{2}\right) \frac{E_2 h^3}{a^4 q_0}$
10	$K_1 = 0, K_2 = 0$	This study 8×8	1.1876
		This study 12×12	1.2236
		This study 16×16	1.2363
		Setoodeh & Karami, 2004	1.237
	$K_1 = 100, K_2 = 0$	This study 8×8	0.5503
		This study 12×12	0.5537
		This study 16×16	0.5548
		Setoodeh & Karami, 2004	0.5525
	$K_1 = 100, K_2 = 10$	This study 8×8	0.2620
		This study 12×12	0.2638
		This study 16×16	0.2644
		Setoodeh & Karami, 2004	0.2679

4.1.2. Nonlinear problems

4.1.2.1. The rectangular composite plates

In this subsection, we study the nonlinear displacement response ($w^* = w/h$) of a composite square plate $a = b$, four layers ($0^\circ/90^\circ/90^\circ/0^\circ$) with SSSS1 boundary conditions under uniform loading condition $P = \frac{qa^4}{E_2 h^4}$. The material parameters of the plate are as follows: $E_1 = 25, E_2 = 1, G_{12} = G_{13} = 0.5E_2, \nu_{12} = 0.25, G_{23} = 0.2E_2$. The composite square plate is divided into a 10×10 mesh for computation. **Table 4** presents a comparison of the nonlinear displacement results of the composite plate using the present model with other studies, including Kant & Kommineni, 1992, who used the FEM based on HSDT, Nguyen-Van et al., 2014, who used the FEM relied on FSDT, and Zhang and Kim (2006), who used four-node elements RDKQ-NL20 and RDKQ-NL24. Additionally, Fig. 4 shows a comparison of the displacement response of the present method with the study by Kant & Kommineni, 1992. Observing the tables and figures, it can be seen that the present study is in good agreement with the published studies, those using HSDT. In particular, the results are very close to those obtained by the MISQ method, which also used a 10×10 mesh. Moreover, when the plate becomes thinner ($h/a = 40$), the results from the current method remain in very good agreement with the aforementioned studies, demonstrating that the proposed element effectively eliminates shear locking.

Table 4. Dimensionless displacement of the composite plate

a/h	P	HOST (Kant & Kommineni, 1992)	MISQ (Nguyen-Van et al., 2014)	NL20 (Zhang & Kim, 2006)	NL24 (Zhang & Kim, 2006)	Present
10	50	0.360	0.356	0.363	0.370	0.3507
	100	0.520	0.521	0.514	0.525	0.5109
	150	0.624	0.629	0.616	0.629	0.6164
	200	0.696	0.711	0.695	0.71	0.6971
	250	0.760	0.779	0.761	0.777	0.7636
20	50	0.320	0.312	0.323	0.327	0.3071
	100	0.493	0.487	0.487	0.494	0.4770
	150	0.592	0.603	0.597	0.608	0.5907
	200	0.680	0.691	0.682	0.695	0.6777
	250	0.752	0.765	0.751	0.766	0.7489
40	50	0.293	0.296	0.291	0.294	0.2913
	100	0.464	0.473	0.461	0.467	0.4632
	150	0.582	0.592	0.577	0.587	0.5800
	200	0.664	0.683	0.667	0.679	0.6694
	250	0.738	0.759	0.740	0.754	0.7426

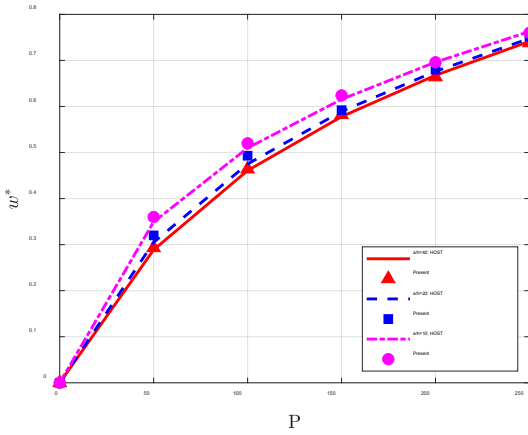


Fig. 4. Comparison of nonlinear displacement response between the present model and the HOST model.

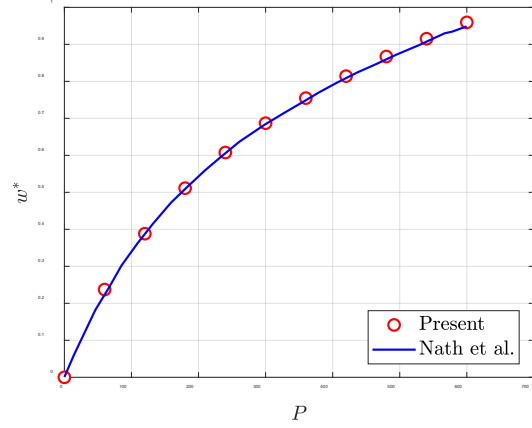


Fig. 5. Dimensionless displacement of the composite plate on an elastic foundation

Fig. 5 presents a comparison of the nonlinear displacement results of the composite plate from the current method with the results of Nath et al., 2006. The geometric dimensions of the plate are $a = b, \frac{a}{h} = 10$; The composite plate with four layer ($0^\circ/90^\circ/0^\circ/90^\circ$), the material parameters of the plate are $E_1 = 25, E_2 = 1, G_{12} = G_{13} = 0.5E_2, \nu_{12} = 0.25, G_{23} = 0.2E_2$. The applied load is $P = \frac{qa^4}{E_2h^4}, w^* = w/h$. The plate has full clamped boundary on four edges. The elastic foundation parameters are $K_1 = 100, K_2 = 0$ and the plate is discretized into a 16×16 mesh. From this figure, we can observe that the current study's results are very close to those of Nath et al., 2006. Through the comparative examples above, It is observed that the results of the current study are accurate and reliable for conducting further investigations with 16×16 mesh.

4.1.2.2. The circular composite plates

This section examines the geometrically nonlinear behavior of a circular plate under uniform pressure. The analysis considers a plate with specific geometric properties, including a radius-to-thickness ratio of $R/h = 50$, and material characteristics such as Young's modulus $E = 10^7$ and Poisson's ratio $\nu = 0.3$. The circular plate is divided into 143 elements and 87 nodes as shown in the Fig. 6 for computation. The transverse central displacements obtained using the current method, as presented in Table 5, are compared to the analytical solution (Weil & Newmark, 1956). Additionally, comparisons are made with RNEM (Zhang & Cheung, 2003), as well as Mindlin-based models such as the nine-node Lagrangian quadrilateral element (QL) (Pica et al., 1980) and the mixed interpolation smoothing quadrilateral element (MISQ20) (Nguyen-Van et al., 2014). By comparing the studies mentioned above, It may be noticed that the results of the proposed method align well with all the studies.

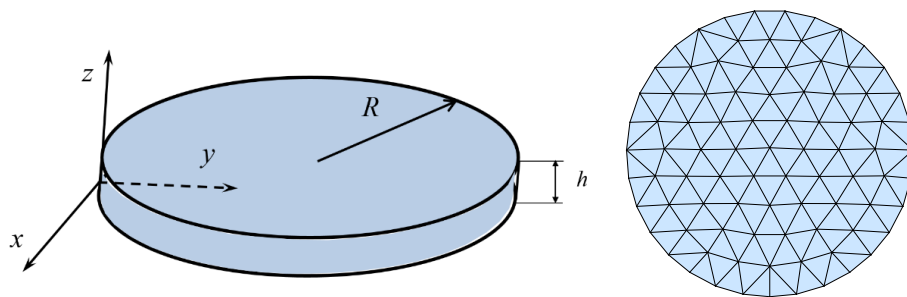


Fig. 6. Mesh model for circular plates

Table 5. Nondimension central displacement of a clamped circular plate under uniform load

Load \bar{P}	MISQ20 (Nguyen-Van et al., 2014)	QL Pica et al., 1980	RNEM (Zhang & Cheung, 2003)	Current work	Analysis solution (Weil & Newmark, 1956)
1	0.170	0.1682	0.1664	0.1668	0.169
2	0.327	0.3231	0.3179	0.3227	0.323
3	0.465	0.4591	0.4514	0.4624	0.457
6	0.780	0.7702	0.7637	0.7585	0.761
10	1.067	1.0514	1.0544	1.0671	1.035
15	1.320	1.3007	1.3164	1.3250	1.279

4.2. Parameter study

4.2.1. The rectangular BiHLC plates

In this subsection, we investigate the nonlinear displacement of a rectangular BiHLC plate. The plate dimensions are $a = b$, $\frac{a}{h} = 10$, and the material parameters of the plate are $E_1 = 25$, $E_2 = 1$, $G_{12} = G_{13} = 0.5E_2$, $\nu_{12} = 0.25$, $G_{23} = 0.2E_2$. The uniform distributed load (UDL) is $P = \frac{qa^4}{E_2h^4}$, $w^* = w/h$. Fig. 7 illustrates the linear and nonlinear displacement of the BiHLC plate with a unidirectional (UD) layer configuration and clamped boundary conditions on all four edges. It is evident that the displacements in both linear and nonlinear cases differ significantly. These results suggest that engineers should carefully consider whether to account for geometric nonlinearity in the structure depending on the specific circumstances.

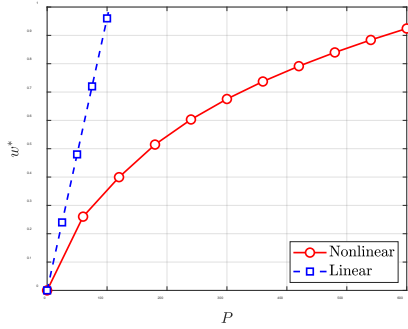


Fig. 7. Comparison of the nondimensional central deflection of BiHLC plates

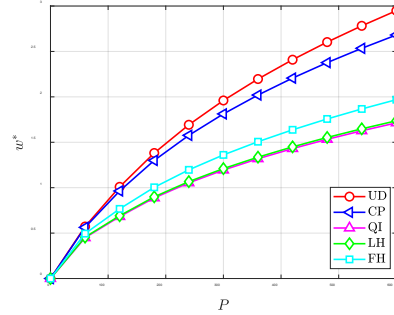


Fig. 8. The nondimensional central deflection of BiHLC plates with the layers

Next, we investigate the nonlinear displacement of a simply supported (SSSS) BiHLC plate with different layup configurations, including UD, CP, QI, LH, and FH, as presented in Fig. 8. From these images, it can be observed that the UD layup configuration results in the largest displacement of the plate, while the QI case shows the smallest displacement. It is noted that the QI and LH configurations exhibit nearly identical displacement responses. This similarity occurs because both laminates provide nearly isotropic overall stiffness. The QI layup distributes fiber orientations uniformly within the plane (0° , $\pm 45^\circ$, 90°), while the LH layup features a gradual and symmetric variation of fiber angles through the thickness. Although their stacking patterns differ, the averaged in-plane and bending stiffness of the LH laminate are very close to those of the QI laminate. As a result, both laminates show almost the same bending and deflection behavior under both linear and nonlinear conditions.

Table 6. The nonlinear central deflection of square BiHLC plates with difference load

P	K_1, K_2	UD	CP	QI	LH	FH
60	0,0	0.5651	0.5553	0.4443	0.4505	0.4890
	100,0	0.3367	0.3425	0.2951	0.2979	0.3133
	100,10	0.1926	0.1934	0.1770	0.1779	0.1832
120	0,0	0.9979	0.9535	0.6758	0.6847	0.7596
	100,0	0.6519	0.6525	0.5219	0.5272	0.5659
	100,10	0.3825	0.3830	0.3420	0.3441	0.3572
180	0,0	1.3661	1.2874	0.8786	0.8902	0.9944
	100,0	0.9453	0.9337	0.7144	0.7220	0.7835
	100,10	0.5691	0.5678	0.4952	0.4984	0.5214
240	0,0	1.6725	1.5608	1.0411	1.0549	1.1840
	100,0	1.2123	1.1825	0.8745	0.8841	0.9673
	100,10	0.7506	0.7458	0.6339	0.6384	0.6730
300	0,0	1.9356	1.7938	1.1786	1.1943	1.3450
	100,0	1.4547	1.4040	1.0121	1.0236	1.1269
	100,10	0.9262	0.9159	0.7593	0.7652	0.8123
360	0,0	2.1671	1.9981	1.2989	1.3164	1.4864
	100,0	1.6758	1.6033	1.1335	1.1468	1.2685
	100,10	1.0952	1.0778	0.8734	0.8805	0.9407
420	0,0	2.3747	2.1813	1.4066	1.4256	1.6129
	100,0	1.8787	1.7846	1.2427	1.2575	1.3963
	100,10	1.2575	1.2317	0.9780	0.9863	1.0594
480	0,0	2.5636	2.3480	1.5042	1.5246	1.7278
	100,0	2.0662	1.9513	1.3423	1.3585	1.5132
	100,10	1.4132	1.3778	1.0745	1.0841	1.1698
540	0,0	2.7374	2.5016	1.5937	1.6154	1.8332
	100,0	2.2406	2.1058	1.4339	1.4515	1.6210
	100,10	1.5624	1.5166	1.1643	1.1750	1.2730
600	0,0	2.8987	2.6444	1.6763	1.6992	1.9306
	100,0	2.4037	2.2501	1.5189	1.5377	1.7211
	100,10	1.7055	1.6488	1.2483	1.2602	1.3701

Table 6 present the nonlinear displacement response of the SSSS BiHLCo plate with different layer configurations on an elastic medium. This table examines the elastic foundation using the Winkler model ($K_1 = 100$), and the Pasternak model ($K_1 = 100, K_2 = 10$). Observing these figures, we can see that the presence of an elastic medium reduces the displacement response, specifically by about 20% for the Winkler model and over 40% for the Pasternak model. Based on these observations, engineers can increase the stiffness of the plate by adjusting the elastic foundation with different stiffness coefficients according to practical requirements. Fig. 9 presents the dimensionless displacement response of the BiHLCo plate on an elastic foundation with different boundary conditions, including SSSS, CCCC, SCSC, CCSS, and SSSC. From this figure, It may be noticed that the SSSS boundary condition results in the largest displacement response, while the CCCC boundary condition results in the smallest displacement response. This is because the CCCC boundary condition always provides the highest rigidity to the plate.

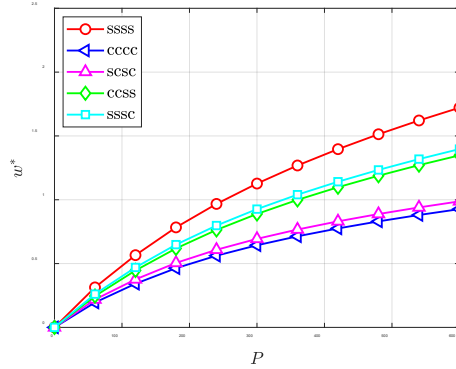


Fig. 9. The nonlinear central deflection of BiHLCo plates with different boundary conditions ($K_1 = 100, K_2 = 0$)

4.2.2. The circular BiHLCo plates

In this subsection, we investigate the nonlinear displacement of a circular BiHLCo plate. The plate dimensions are $R = 1$, $\frac{R}{h} = 10$, and the material parameters of the circular plate are $E_1 = 25, E_2 = 1, G_{12} = G_{13} = 0.5E_2, \nu_{12} = 0.25, G_{23} = 0.2E_2$. The uniform distributed load (UDL) is $P = \frac{qa^4}{E_2h^4}$ and dimensionless deflection $w^* = w/h$. The circular plate has a shape and is meshed as presented in **Fig. 6**. **Fig. 10a** illustrates the nonlinear deflection of circular BiHLCo plates subjected to uniformly distributed load P with various lay-up configurations and fully clamped boundary conditions and **Fig. 10b** is a magnified view of the deflection response curves for different layup configurations. From the figure, it can be observed that, similar to square plates, circular BiHLCo plates also exhibit deflection responses with the UD lay-up configuration.

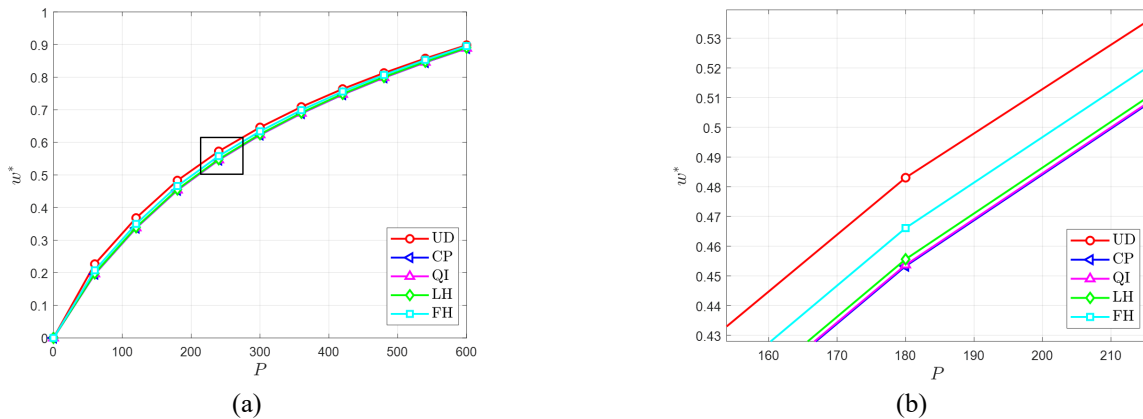


Fig. 10. The nonlinear central deflection of circular BiHLCo plates with the layers

Table 7 presents the central displacement of a BiHLCo circular plate under various loads on an elastic foundation, considering geometric nonlinearity effects. From this table, it is evident that the elastic foundation significantly influences the displacement response of the BiHLCo circular plate. When the foundation stiffness parameters K_1, K_2 are set to 100 and 10, respectively, the plate's displacement decreases substantially. However, the impact of the elastic foundation on displacement is more pronounced under lower loads. For instance, when $P = 60$ and $K_1, K_2 = 100, 10$, the displacement response decreases by nearly 50% compared to when there is no foundation. Conversely, when $P = 600$ with the same stiffness parameters, the displacement response only reduces by about 15% compared to the scenario without an elastic foundation. This clearly shows

that the foundation has a stronger influence at lower loads. As the load increases, geometric nonlinearity induces significant in-plane membrane forces that stiffen the plate, thereby diminishing the relative contribution of the foundation stiffness. In physical terms, the membrane effect dominates at high load levels, and the linear stiffness of the foundation becomes less effective in resisting deflection.

Table 7. The nonlinear dimensionless displacement of circular BiHLCo plates with difference load resting on elastic foundation

P	K_1, K_2	UD	CP	QI	LH	FH
60	0,0	0.2267	0.1960	0.1964	0.1980	0.2076
	100,0	0.1782	0.1594	0.1597	0.1608	0.1669
	100,10	0.1191	0.1114	0.1116	0.1121	0.1147
120	0,0	0.3681	0.3373	0.3376	0.3395	0.3499
	100,0	0.3133	0.2897	0.2901	0.2915	0.2997
	100,10	0.2273	0.2145	0.2147	0.2156	0.2200
180	0,0	0.4830	0.4533	0.4537	0.4556	0.4661
	100,0	0.4252	0.4005	0.4009	0.4026	0.4115
	100,10	0.3252	0.3091	0.3095	0.3106	0.3162
240	0,0	0.5725	0.5459	0.5463	0.5481	0.5579
	100,0	0.5154	0.4921	0.4926	0.4943	0.5030
	100,10	0.4111	0.3935	0.3940	0.3952	0.4014
300	0,0	0.6461	0.6228	0.6232	0.6250	0.6339
	100,0	0.5905	0.5696	0.5701	0.5718	0.5799
	100,10	0.4865	0.4686	0.4691	0.4704	0.4768
360	0,0	0.7088	0.6887	0.6891	0.6908	0.6988
	100,0	0.6550	0.6366	0.6372	0.6388	0.6462
	100,10	0.5531	0.5357	0.5362	0.5375	0.5439
420	0,0	0.7637	0.7466	0.7470	0.7486	0.7558
	100,0	0.7117	0.6958	0.6964	0.6979	0.7046
	100,10	0.6127	0.5960	0.5966	0.5979	0.6041
480	0,0	0.8129	0.7983	0.7988	0.8004	0.8067
	100,0	0.7624	0.7488	0.7494	0.7509	0.7570
	100,10	0.6665	0.6509	0.6514	0.6527	0.6587
540	0,0	0.8574	0.8452	0.8457	0.8473	0.8529
	100,0	0.8084	0.7970	0.7976	0.7991	0.8044
	100,10	0.7156	0.7010	0.7016	0.7029	0.7085
600	0,0	0.8983	0.8883	0.8888	0.8903	0.8952
	100,0	0.8506	0.8412	0.8418	0.8433	0.8480
	100,10	0.7607	0.7473	0.7479	0.7492	0.7545

4.3. The feedforward ANN model for bending analysis of BiHLCo plates

In this study, a feedforward ANN model is developed to rapidly estimate the nonlinear central displacement of BiHLCo plates resting on a Pasternak foundation under varying load conditions. A dataset containing input parameters and corresponding nonlinear displacements is used to train an ANN. The proposed model follows these key steps:

Data Collection and Preprocessing

The dataset is constructed from **Table 6**, containing nonlinear displacement results for different load values and foundation stiffness parameters. The dataset includes:

- Inputs: Load (P), Pasternak foundation stiffness parameters (K_1, K_2)
- Outputs: Nonlinear central displacement values corresponding to different fiber orientations (UD, CP, QI, LH, FH).

ANN Architecture

ANN is employed to predict nonlinear displacement. The model architecture consists of:

- Input Layer: Three neurons corresponding to (P, K_1, K_2).
- Hidden Layers: Two fully connected layers with 10 and 8 neurons, respectively.
- Activation Function: Leaky ReLU in hidden layers to enhance nonlinear representation.
- Output Layer: Five neurons corresponding to the displacement values of UD, CP, QI, LH, and FH.

The ANN architecture diagram is illustrated as in **Fig. 11**.

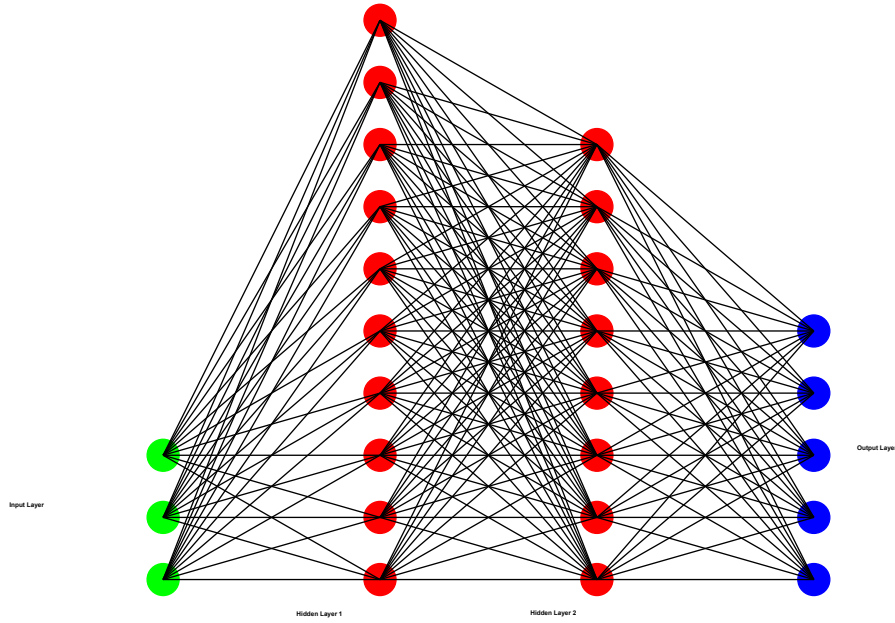


Fig. 11. The ANN architecture diagram

Model Training

The dataset is split into:

- 80% for training
- 20% for testing

The backpropagation algorithm combined with the Levenberg-Marquardt optimization method (Hagan & Menhaj, 1994) is used to minimize the loss function, defined as the mean squared error (MSE):

$$\text{MSE} = \frac{1}{n} \sum_{i=1}^n (w_i - \hat{w}_i)^2 \quad (43)$$

where w_i is the actual displacement and \hat{w}_i is the predicted displacement.

Model Performance Evaluation

The trained ANN model is evaluated on unseen test data, and its accuracy is assessed using the following metrics:

Root Mean Square Error (RMSE):

$$\text{RMSE} = \sqrt{\frac{1}{n} \sum_{i=1}^n (w_i - \hat{w}_i)^2} \quad (44)$$

Coefficient of Determination (\mathbb{R}^2)

$$\mathbb{R}^2 = 1 - \frac{\sum (w_i - \hat{w}_i)^2}{\sum (w_i - \bar{w})^2} \quad (45)$$

where \bar{w} is the mean of actual displacements.

ANN Hyperparameters and Training Details

To enhance reproducibility, all ANN hyperparameters and training settings are summarized below. The model is a feed-forward network trained with the Levenberg–Marquardt (LM) algorithm.

Table 8. Artificial neural network hyperparameters and training settings

Parameter	Description / Value
Architecture	Feedforward neural network
Input neurons	3 (P, K ₁ , K ₂)
Hidden layers	2
Hidden neurons	10 (Layer 1), 8 (Layer 2)
Activation function	Leaky ReLU ($\alpha = 0.01$)
Output neurons	5 (UD, CP, QI, LH, FH)
Training algorithm	Levenberg–Marquardt (LM)
Loss function	Mean Squared Error (MSE)
Epochs	1000
Learning rate	0.001
Training/Test split	80% / 20%
Performance metric	RMSE, R^2
Early stopping	Enabled (patience = 20 epochs)

Model Performance Evaluation

Table 9 reports the final performance on the training and test sets. The low RMSE and R^2 values close to 1.0 indicate strong generalization.

Table 9. Artificial neural network model performance on training and test sets.

Dataset	RMSE	R^2
Training	0.0042	0.9989
Testing	0.0061	0.9974

These results demonstrate that the ANN can accurately predict the nonlinear displacement of BiHLC_o plates with high precision while maintaining robust generalization on unseen data. The results in **Table 10** indicate that the ANN model provides predictions very close to those obtained using the finite element method (the smallest error between the FEM result and the predicted result by ANN is 0.0044%, and the largest error is 1.35%). Based on these findings, it can be concluded that the proposed ANN model in this study is highly reliable and can be further extended for structural parameter optimization. Additionally, it serves as an efficient rapid prediction tool for practical engineering applications, significantly reducing computational time while maintaining high accuracy.

Table 10. Comparison of plate displacement results between FEM and ANN

P (N)	K1	K2	UD (FEM)	CP (FEM)	QI (FEM)	LH (FEM)	FH (FEM)	UD (ANN)	CP (ANN)	QI (ANN)	LH (ANN)	FH (ANN)
60	0	0	0.5651	0.5553	0.4443	0.4505	0.489	0.5670	0.5566	0.4444	0.4502	0.4891
	100	0	0.3367	0.3425	0.2951	0.2979	0.3133	0.3400	0.3452	0.2952	0.2978	0.3136
	100	10	0.1926	0.1934	0.177	0.1779	0.1832	0.1977	0.1967	0.1780	0.1789	0.1845
120	0	0	0.9979	0.9535	0.6758	0.6847	0.7596	0.9989	0.9540	0.6757	0.6847	0.7597
	100	0	0.6519	0.6525	0.5219	0.5272	0.5659	0.6547	0.6548	0.5219	0.5270	0.5660
	100	10	0.3825	0.383	0.342	0.3441	0.3572	0.3865	0.3859	0.3429	0.3450	0.3584
180	0	0	1.3661	1.2874	0.8786	0.8902	0.9944	1.3660	1.2871	0.8782	0.8898	0.9939
	100	0	0.9453	0.9337	0.7144	0.722	0.7835	0.9473	0.9356	0.7145	0.7218	0.7836
	100	10	0.5691	0.5678	0.4952	0.4984	0.5214	0.5724	0.5701	0.4957	0.4991	0.5223
240	0	0	1.6725	1.5608	1.0411	1.0549	1.184	1.6720	1.5606	1.0423	1.0561	1.1848
	100	0	1.2123	1.1825	0.8745	0.8841	0.9673	1.2151	1.1842	0.8704	0.8799	0.9642
	100	10	0.7506	0.7458	0.6339	0.6384	0.673	0.7519	0.7461	0.6336	0.6383	0.6727
300	0	0	1.9356	1.7938	1.1786	1.1943	1.345	1.9332	1.7918	1.1781	1.1939	1.3442
	100	0	1.4547	1.404	1.0121	1.0236	1.1269	1.4548	1.4035	1.0071	1.0186	1.1223
	100	10	0.9262	0.9159	0.7593	0.7652	0.8123	0.9278	0.9167	0.7595	0.7655	0.8124
360	0	0	2.1671	1.9981	1.2989	1.3164	1.4864	2.1649	1.9962	1.2979	1.3155	1.4852
	100	0	1.6758	1.6033	1.1335	1.1468	1.2685	1.6745	1.6027	1.1332	1.1464	1.2681
	100	10	1.0952	1.0778	0.8734	0.8805	0.9407	1.0955	1.0781	0.8730	0.8804	0.9406
420	0	0	2.3747	2.1813	1.4066	1.4256	1.6129	2.3721	2.1791	1.4057	1.4247	1.6118
	100	0	1.8787	1.7846	1.2427	1.2575	1.3963	1.8771	1.7839	1.2421	1.2569	1.3957
	100	10	1.2575	1.2317	0.978	0.9863	1.0594	1.2433	1.2200	0.9723	0.9808	1.0536
480	0	0	2.5636	2.348	1.5042	1.5246	1.7278	2.5607	2.3455	1.5032	1.5236	1.7266
	100	0	2.0662	1.9513	1.3423	1.3585	1.5132	2.0647	1.9502	1.3416	1.3576	1.5123
	100	10	1.4132	1.3778	1.0745	1.0841	1.1698	1.3817	1.3515	1.0640	1.0736	1.1582
540	0	0	2.7374	2.5016	1.5937	1.6154	1.8332	2.7348	2.4994	1.5926	1.6144	1.8319
	100	0	2.2406	2.1058	1.4339	1.4515	1.621	2.2508	2.1140	1.4455	1.4628	1.6324
	100	10	1.5624	1.5166	1.1643	1.175	1.273	1.5423	1.5001	1.1595	1.1702	1.2676
600	0	0	2.8987	2.6444	1.6763	1.6992	1.9306	2.8576	2.6099	1.6565	1.6790	1.9054
	100	0	2.4037	2.2501	1.5189	1.5377	1.7211	2.4319	2.2707	1.5475	1.5659	1.7493
	100	10	1.7055	1.6488	1.2483	1.2602	1.3701	1.7052	1.6486	1.2481	1.2599	1.3698

5. Conclusion

This paper introduces, for the first time, an analysis of nonlinear static bending in BiHLC_o plates supported by a two-parameter Pasternak elastic foundation, utilizing the finite element method. The MITC3i element, based on FSDT, is employed to model and solve the governing equations. To validate the proposed model, the results are compared with available data from the literature. The key conclusions from the study are summarized below:

- The paper provides several results on the nonlinear deflection of BiHLC_o plates with various lay-up configurations, which engineers can apply in practical scenarios.
- The deflection responses obtained using Winkler or Pasternak elastic foundations are also significant for engineers in designing and applying foundation structures in real-world engineering.
- The MITC3i triangular element demonstrates good accuracy and performs well in meshing complex structures.
- It was observed that the proposed MITC3i element effectively captures large deflection behavior for both rectangular and circular BiHLC_o plates, with the numerical results showing excellent agreement with benchmark studies. The element also shows no shear-locking issues, even for thin plates, and achieves less than 1% deviation from Mohamed et al. [26] using a 16×16 mesh, confirming its reliability and convergence.
- The influence of the elastic foundation was also clarified. The foundation greatly reduces the deflection under low loads, whereas its effect becomes less significant at higher loads due to geometric nonlinearity and the dominance of membrane forces in the in-plane stiffness.
- The comparison among different layup configurations revealed that QI and LH laminates exhibit nearly identical global responses due to their similar isotropic stiffness characteristics, suggesting that LH can be used as a cost-effective alternative to QI without loss of accuracy.

The novelty of this study:

- The MITC3i element is appropriate for investigating nonlinear behavior in bio-inspired composite structures.
- An ANN-based predictive approach for efficiently computing the nonlinear displacement of BiHLC_o plates are proposed to help significantly reduce computation time while maintaining accuracy.
- The developed ANN model achieved a maximum deviation of less than 1.35% compared with FEM results, allowing near-instantaneous prediction of displacement without executing the FEM computation.
- The results of this paper will serve as a benchmark for future studies to compare computational results for BiHLC_o plate structures.

Conflicts of Interest

The authors declare that there are no financial interests or personal relationships that could have influenced the findings presented in this paper.

Data availability

The data supporting the results of this study will be made available upon request.

References

- Amara, R., Riadh, B., Hassen, A. A., Mokhtar, N., & Hadji, L. (2024). Hygrothermal effect of bio-inspired helicoid laminate plate for strengthening damaged RC beam. *Mechanics of Advanced Materials and Structures*, 1-18. doi:10.1080/15376494.2024.2392623
- Barbero, E. J. (2011). *Introduction to Composite Materials Design*. Boca Raton: CRC Press.
- Benyus, J. (1997). *Innovation inspired by nature: Biomimicry*. New York: William Morrow & Co.
- Bischoff, M., & Bletzinger, K.-U. (2004). Improving stability and accuracy of Reissner–Mindlin plate finite elements via algebraic subgrid scale stabilization. *Computer Methods in Applied Mechanics and Engineering*, 193(15-16), 1517-1528. doi:10.1016/j.cma.2003.12.036
- Cui, X. Y., & Tian, L. (2017). A Central Point-Based Discrete Shear Gap Method for Plates and Shells Analysis Using Triangular Elements. *International Journal of Applied Mechanics*, 09(04). doi:10.1142/s1758825117500557
- Do, N.-T., Nguyen, T. T., Tran, T. T., Le, P. B., & Pham, Q.-H. (2023). Free vibration analysis of bio-inspired helicoid laminated composite plates resting on elastic foundation using isogeometric analysis and artificial neural network. *Mechanics of Time-Dependent Materials*, 28(4), 2487-2510. doi:10.1007/s11043-023-09649-1
- Fadlallah, S. O., Anderson, T. N., & Nates, R. J. (2021). Artificial Neural Network–Particle Swarm Optimization (ANN-PSO) Approach for Behaviour Prediction and Structural Optimization of Lightweight Sandwich Composite Heliostats. *Arabian Journal for Science and Engineering*, 46(12), 12721-12742. doi:10.1007/s13369-021-06126-0
- Garg, A., Belarbi, M.-O., Li, L., Sharma, N., Gupta, A., & Chalak, H. D. (2023). Free vibration analysis of bio-inspired helicoid laminated composite plates. *The Journal of Strain Analysis for Engineering Design*, 58(7), 538-548. doi:10.1177/03093247231160414

- Hagan, M. T., & Menhaj, M. B. (1994). Training feedforward networks with the Marquardt algorithm. *IEEE Trans Neural Netw*, 5(6), 989-993. doi:10.1109/72.329697
- Kant, T., & Kommineni, J. R. (1992). C0 Finite element geometrically non-linear analysis of fibre reinforced composite and sandwich laminates based on a higher-order theory. *Computers & Structures*, 45(3), 511-520. doi:10.1016/0045-7949(92)90436-4
- Karamanli, A., Vo, T. P., & Eltaher, M. A. (2024). Comprehensive analysis of bio-inspired laminated composites plates using a quasi-3D theory and higher order FE models. *Thin-Walled Structures*, 198. doi:10.1016/j.tws.2024.111735
- Khatir, S., Tiachacht, S., Le Thanh, C., Ghandourah, E., Mirjalili, S., & Abdel Wahab, M. (2021). An improved Artificial Neural Network using Arithmetic Optimization Algorithm for damage assessment in FGM composite plates. *Composite Structures*, 273. doi:10.1016/j.compstruct.2021.114287
- Lee, P.-S., & Bathe, K.-J. (2004). Development of MITC isotropic triangular shell finite elements. *Computers & Structures*, 82(11-12), 945-962. doi:10.1016/j.compstruc.2004.02.004
- Lee, P.-S., & Bathe, K.-J. (2010). The quadratic MITC plate and MITC shell elements in plate bending. *Advances in Engineering Software*, 41(5), 712-728. doi:10.1016/j.advengsoft.2009.12.011
- Lee, Y., Jeon, H.-M., Lee, P.-S., & Bathe, K.-J. (2015). The modal behavior of the MITC3+ triangular shell element. *Computers & Structures*, 153, 148-164. doi:10.1016/j.compstruc.2015.02.033
- Lee, Y., Lee, P.-S., & Bathe, K.-J. (2014). The MITC3+ shell element and its performance. *Computers & Structures*, 138, 12-23. doi:10.1016/j.compstruc.2014.02.005
- Mahesh, V. (2023). Artificial neural network (ANN) based investigation on the static behaviour of piezo-magneto-thermo-elastic nanocomposite sandwich plate with CNT agglomeration and porosity. *International Journal of Non-Linear Mechanics*, 153. doi:10.1016/j.ijnonlinmec.2023.104406
- Mohamed, S. A., Mohamed, N., & Eltaher, M. A. (2022a). Bending, buckling and linear vibration of bio-inspired composite plates. *Ocean Engineering*, 259. doi:10.1016/j.oceaneng.2022.111851
- Mohamed, S. A., Mohamed, N., & Eltaher, M. A. (2022b). Bending, buckling and linear vibration of bio-inspired composite plates. *Ocean Engineering*, 259, 111851. doi:10.1016/j.oceaneng.2022.111851
- Mohammad Malekzadeh, S. H.-J., Saeed Shojaee (2021). Improvement of Numerical Manifold Method using Nine-node Quadrilateral and Ten-node Triangular Elements along with Complex Fourier RBFs in Modeling Free and Forced Vibrations. *Journal of Applied and Computational Mechanics*, 7(4), 2049-2063. doi:10.22055/jacm.2020.32423.2027
- Nath, Y., Prithviraju, M., & Mufti, A. A. (2006). Nonlinear statics and dynamics of antisymmetric composite laminated square plates supported on nonlinear elastic subgrade. *Communications in Nonlinear Science and Numerical Simulation*, 11(3), 340-354. doi:10.1016/j.cnsns.2004.11.003
- Nguyen-Van, H., Nguyen-Hoai, N., Chau-Dinh, T., & Nguyen-Thoi, T. (2014). Geometrically nonlinear analysis of composite plates and shells via a quadrilateral element with good coarse-mesh accuracy. *Composite Structures*, 112, 327-338. doi:10.1016/j.compstruct.2014.02.024
- Nguyen, T.-K., Nguyen, V.-H., Chau-Dinh, T., Vo, T. P., & Nguyen-Xuan, H. (2016). Static and vibration analysis of isotropic and functionally graded sandwich plates using an edge-based MITC3 finite elements. *Composites Part B: Engineering*, 107, 162-173. doi:10.1016/j.compositesb.2016.09.058
- Pawlyn, M. (2019). *Biomimicry in Architecture*. London: RIBA Publishing.
- Pham, Q.-H., Nguyen, P.-C., & Tran, T. T. (2022a). Free vibration response of auxetic honeycomb sandwich plates using an improved higher-order ES-MITC3 element and artificial neural network. *Thin-Walled Structures*, 175. doi:10.1016/j.tws.2022.109203
- Pham, Q.-H., Pham, T.-D., Trinh, Q. V., & Phan, D.-H. (2019). Geometrically nonlinear analysis of functionally graded shells using an edge-based smoothed MITC3 (ES-MITC3) finite elements. *Engineering with Computers*, 36(3), 1069-1082. doi:10.1007/s00366-019-00750-z
- Pham, Q.-H., Thanh Tran, T., Ke Tran, V., Nguyen, P.-C., & Nguyen-Thoi, T. (2022b). Free vibration of functionally graded porous non-uniform thickness annular-nanoplates resting on elastic foundation using ES-MITC3 element. *Alexandria Engineering Journal*, 61(3), 1788-1802. doi:10.1016/j.aej.2021.06.082
- Pham, Q.-H., Tran, V. K., & Tran, T. T. (2023). Vibration characteristics of sandwich plates with an auxetic honeycomb core and laminated three-phase skin layers under blast load. *Defence Technology*, 24, 148-163. doi:10.1016/j.dt.2022.10.002
- Pica, A., Wood, R. D., & Hinton, E. (1980). Finite element analysis of geometrically nonlinear plate behaviour using a mindlin formulation. *Computers & Structures*, 11(3), 203-215. doi:10.1016/0045-7949(80)90160-1
- Reddy, J. N. ((2003)). *Mechanics of laminated composite plates and shells: theory and analysis*: CRC press.
- Ribeiro Junior, R. F., & Gomes, G. F. (2023). On the Use of Machine Learning for Damage Assessment in Composite Structures: A Review. *Applied Composite Materials*, 31(1), 1-37. doi:10.1007/s10443-023-10161-5
- Setoodeh, A. R., & Karami, G. (2004). Static, free vibration and buckling analysis of anisotropic thick laminated composite plates on distributed and point elastic supports using a 3-D layer-wise FEM. *Engineering Structures*, 26(2), 211-220. doi:10.1016/j.engstruct.2003.09.009
- Sharma, A., Belarbi, M. O., Garg, A., & Li, L. (2023). Bending analysis of bio-inspired helicoidal/Bouligand laminated composite plates. *Mechanics of Advanced Materials and Structures*, 31(21), 5326-5340. doi:10.1080/15376494.2023.2214934
- Weil, N. A., & Newmark, N. M. (1956). Large Deflections of Elliptical Plates. *Journal of Applied Mechanics*, 23(1), 21-26. doi:10.1115/1.4011202

- Zhang, Y. X., & Cheung, Y. K. (2003). Geometric nonlinear analysis of thin plates by a refined nonlinear non-conforming triangular plate element. *Thin-Walled Structures*, 41(5), 403-418. doi:10.1016/s0263-8231(02)00114-3
- Zhang, Y. X., & Kim, K. S. (2006). Geometrically nonlinear analysis of laminated composite plates by two new displacement-based quadrilateral plate elements. *Composite Structures*, 72(3), 301-310. doi:10.1016/j.compstruct.2005.01.001



© 2026 by the authors; licensee Growing Science, Canada. This is an open access article distributed under the terms and conditions of the Creative Commons Attribution (CC-BY) license (<http://creativecommons.org/licenses/by/4.0/>).